



A micro-tattooing device for capsule endoscope using a Wood's metal triggering mechanism[☆]

Seonggun Joe^{a,b,c,1}, Dongkyu Lee^{a,1}, Hyeongseok Kang^a, Byungjeon Kang^d, Jong-Oh Park^{d,*},
Byungkyu Kim^{a,*}

^a School of Aerospace and Mechanical Engineering, Korea Aerospace University, Goyang-si, Republic of Korea

^b Center for Micro-BioRobotics, Istituto Italiano di Tecnologia (IIT), Pontedera, Italy

^c The BioRobotics Institute, Scuola Superiore Sant'Anna, Pontedera, Italy

^d School of Mechanical Engineering, Chonnam National University, Gwangju, Republic of Korea

ARTICLE INFO

Keywords:

Capsule endoscope
Endoscopic tattooing
Colonoscopy
Triggering mechanism
Wood's metal
Liquid metal
Conical spring

ABSTRACT

The endoscopic tattooing procedure is essential before surgery in the gastroenterology practice. Because conventional tattooing is conducted by injecting biocompatible ink from outside the human body, a conventional tattooing device is not appropriate for use in the Capsule Endoscope (CE). A compact micro-tattooing device with an optimal triggering mechanism which can be enclosed in the CE is required. Therefore, A micro-tattooing device operated by two conical springs with a Wood's metal-based triggering module is proposed. Needle insertion and ink injection to the submucosal layer of the colon is actuated by triggering mechanism #1. When triggering mechanism #2 is activated, the needle is withdrawn to avoid scratching the internal lumen. Each triggering module is activated by the Joule heating of a Ni-Cr wire with low power consumption to accommodate the CE battery's small capacity. The in-vitro and ex-vivo tests were conducted to confirm the feasibility of the tattooing module. In the in-vitro test, the needle displacement was confirmed to be 3.3 mm. Using extracted porcine colon, the total tattooing procedure was conducted, and the injected ink in the submucosal layer was observed by hemisectioning the specimen. Conclusively, the device achieved competitive results, both in terms of power consumption and space constraints.

1. Introduction

Since the Capsule Endoscope (CE) has been introduced in 2001 to detection of small-bowel disease [1], various types of CE (e.g. PillCam, EndoCapsule, Olympus, IntroMedic) are successfully commercialized so far [2]. Such the CE is controllable by external control system and is miniaturized to be swallowable. Accordingly, due to its significant advantage of preventing patient's discomfort or pain [3], the CE has emerged as a next generation endoscopic device, which is expected to replace the conventional endoscope in the near future. Recently, advanced researchers developed and presented a pain-free, biocompatible CE made with a soft material, replacing the rigid exterior material of earlier CE designs [4]. Similarly, inspired by collaborative works in academia and the industry, innovative and novel technologies for improving CE have been studied for various applications such as motion control or disease detection techniques. (e.g. Locomotive CE, Electromagnetic actuation (EMA) system, deep convolutional neural network-based disease detection

[5–11]). Despite such technological advances, there are some limitations in the CE's passive diagnostic functions. Because the conventional medical apparatuses can perform both treatment and diagnostic functions, the CE requires the various treatment functions as well such as biopsy and drug delivery module to completely replace the conventional tools. Accordingly, previous researchers have studied the feasibility and compatibility of additional functional modules such as biopsy and drug delivery [5]. Le, et al. presented a biopsy module for the CE, and it was installed in an active locomotive intestinal capsule endoscope [12]. They proposed a novel biopsy mechanism using an electromagnetic field and performed an ex-vivo test in a porcine colon. Similarly, Woods, et al. presented a drug delivery mechanism, which directly injects the drug into the gastrointestinal tract [13,14]. Drug release techniques using a magnetic field have also been presented [15,16].

The major objective of conventional endoscopic tattooing is to detect tumor or polyps on a colon wall and leave a mark at near them, allowing them to be quickly located and removed during a minimally invasive

[☆] This paper was recommended for publication by Associate Editor Bijan Shirinzadeh.

* Corresponding authors.

E-mail addresses: jop@jnu.ac.kr (J.-O. Park), bkim@kau.ac.kr (B. Kim).

¹ These authors contributed equally to this work.

Table 1
Requirements and constrains for the tattooing mechanism and CE for ALICE.

Requirements	Tattooing mechanism	CE for ALICE
Diameter [mm]	11	11
Length [mm]	10	30
Penetrated depth [mm]	<5	–
Available ink cartridge [ml]	0.25	–
Kinematic constrains	45° insertion angle	5 Degrees of Freedom
Assigned battery capacity [mWh]	71.25 (Max. 15%)	475

surgery procedure, such as laparoscopy [17–20]. Many researchers have addressed the issues related with implementation of tattooing mechanism for CE, however, only a few researches have been reported. Hoang, manh cuong, et al. presented a tattooing mechanism that can not only be adapted for use in CE, but also actuated by an external controlling system (EMA system). Interestingly, both the insertion of needle and the injection of ink were actuated along the longitudinal axis of the CE [21].

Meanwhile, in our previous study, we proposed a prototype that was an endoscopic tattooing device for CE [22]. The components of the proposed tattooing mechanism consist of an acrylic post with a screw thread, a nylon cable, and a Ni-Cr and SMA wire. The first triggering mechanism was designed, which was operated by the melting of acrylic post by an overheated Ni-Cr wire. After the needle mechanism operated, a second triggering mechanism was operated by breaking a meshed nylon cable with a heated SMA wire. The main flaws in this design were that the latching force of the acrylic and nylon cable were insufficient to hold the conical spring in a compressed state, and the nylon cable and acrylic post lacked biocompatibility when they burned or melted. Accordingly, in this paper, we addressed these fatal flaws, and proposed an improved, simple and reliable micro tattooing mechanism. We designed a tattooing mechanism that accommodates the constraints and characteristics of an actual CE, and the environmental conditions of conventional tattooing procedure. First of all, we assume the proposed tattooing device will be integrated into a CE for use in the Active Locomotive Capsule Endoscopy (ALICE), which is controlled by an EMA system [16]. Then, a compact micro tattooing device is designed while addressing size constraints for integration into a CE for ALICE. While considering the CE specifications for the ALICE system, and the mechanical operation and component dimensions of the tattooing mechanism (Table 1), we design a compact micro tattooing device triggered by melting a threaded nut made of Wood's metal. The Wood's metal nut creates a more secure and stable mechanism, and it can be activated by using a small amount of electrical power. The conical spring is designed with a shape and size appropriate for needle movement, and the thread pitch of the Wood's metal nut is determined according to the elastic force of the conical spring. Then, a numerical simulation was performed to evaluate the triggering time for the Wood's metal-based triggering mechanism. Based on our findings from the triggering mechanism design and simulation, the micro-tattooing device was fabricated. Finally, India ink injection performance was evaluated through in-vitro and ex-vivo tests with an extracted porcine colon.

2. Materials and methods

2.1. Design requirements for the tattooing device

Before we determine the specification of the tattooing device, we establish the objectives and mechanism performance criteria, according to the conditions of conventional tattooing procedures as follows:

1. According to typical guidelines of tattooing procedure, the needle insertion angle should be 45°, and the injected India ink should be minimum 0.25 ml [19].
2. Considering the general colon wall thickness [24] and the ink cartridge volume of CE, the maximum needle penetration depth should be 3.3 mm, regardless of CE orientation.

3. Considering the average internal tissue pressure, along with the pressure required for needle insertion and ink injection [25], the conical spring should be designed to have the proper force.
4. The power consumption should be under 15% of total battery capacity and the tattooing mechanism power can be controlled by an on/off reed switch [16].

In summary, the typical guidelines of endoscopic tattooing techniques are that the India ink should be injected into the submucosa layer at a 45° insertion angle [19]. The amount of injected India ink should be between 0.25 to 0.5 ml and the insertion depth should be under 3.3 mm so that the needle does not penetrate colon wall. Then, the needle should be fully withdrawn to its original position to prevent scratching the internal colon wall. The needle should also move longitudinally (parallel to the direction of the camera view) so that the operator can view the target (e.g. polyp, tumor) through the camera. There are also several issues regarding space constraints. A traditional actuator such as a bulky electrical motor that requires a lot of space should be avoided since the size of a commercial CE (11 mm in a diameter, 25~30 mm long) is too small to accommodate both a motor and tattooing ink [3]. In addition, the power consumption of the tattooing mechanism should be minimized to a maximum of 15% of total battery capacity. Numeric values for the main requirements are summarized in Table 1.

2.2. Micro-tattooing device design

As shown in Fig. 1(a), the CE consists of a camera module, a battery, a pair of permanent magnets, an antenna and transmitter, and a tattooing module. Based on the aforementioned requirements, the micro tattooing device is designed as shown Fig. 1(b). The proposed device contains two triggering modules to conduct the endoscopic tattooing procedure. Each triggering module consists of a conical spring, a Wood's metal nut, a spring holder, and a Ni-Cr wire. When the triggering module is initiated, the conical spring moves the spring holder. The tattooing needle and a dummy needle are installed on spring holder #1. A 26G needle is selected, which is commonly used in conventional endoscopic tattooing procedures [23]. The dummy needle is employed to aid in alignment and prevent asymmetric deployment of the conical spring. Conical spring #2 is designed to have a force greater than the elastic force of conical spring #1, which recompresses it and withdraws the needle. The Wood's metal is fabricated into a nut-shape for easy fastening to a threaded post on the spring holder. The Ni-Cr wire melts the Wood's metal, releasing the spring holder and allowing it to move. By employing space-saving components such as conical springs and the Wood's metal triggering mechanism, it's possible to reduce the mechanism size to within 16.908% of the total ALICE volume (Total volume = 2,787 mm³), including a 0.25 ml ink cartridge. On the other hand, the previously assigned volume for a tattooing mechanism design, including an ink cartridge, was 836.1 mm³, amounting to 30% of the total ALICE volume.

2.3. Working principle of the micro-tattooing mechanism

The position and orientation of the proposed tattooing device are controlled by an EMA system in the ALICE system. The EMA system has

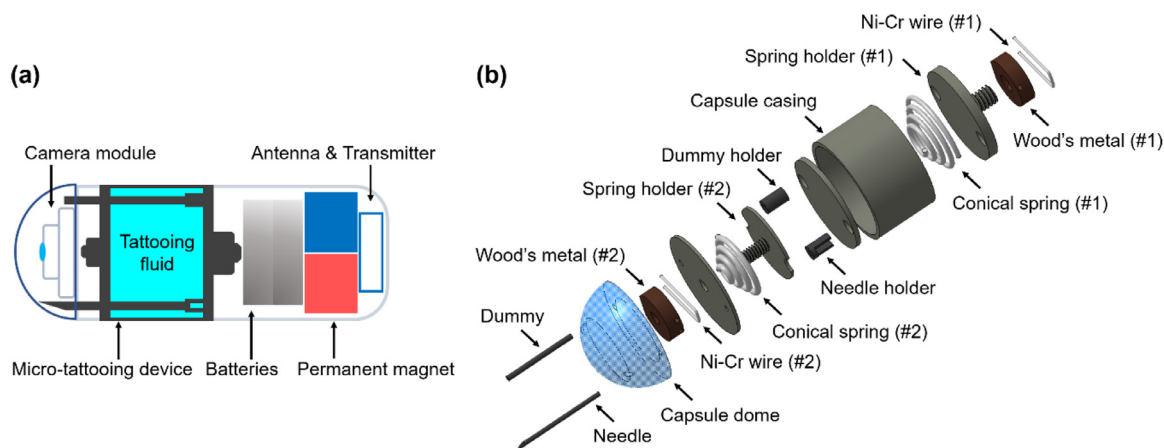


Fig. 1. A scheme of tattooing mechanism for CE (a) Arrangement of components in CE for ALICE (b) Configuration of the micro-tattooing device.

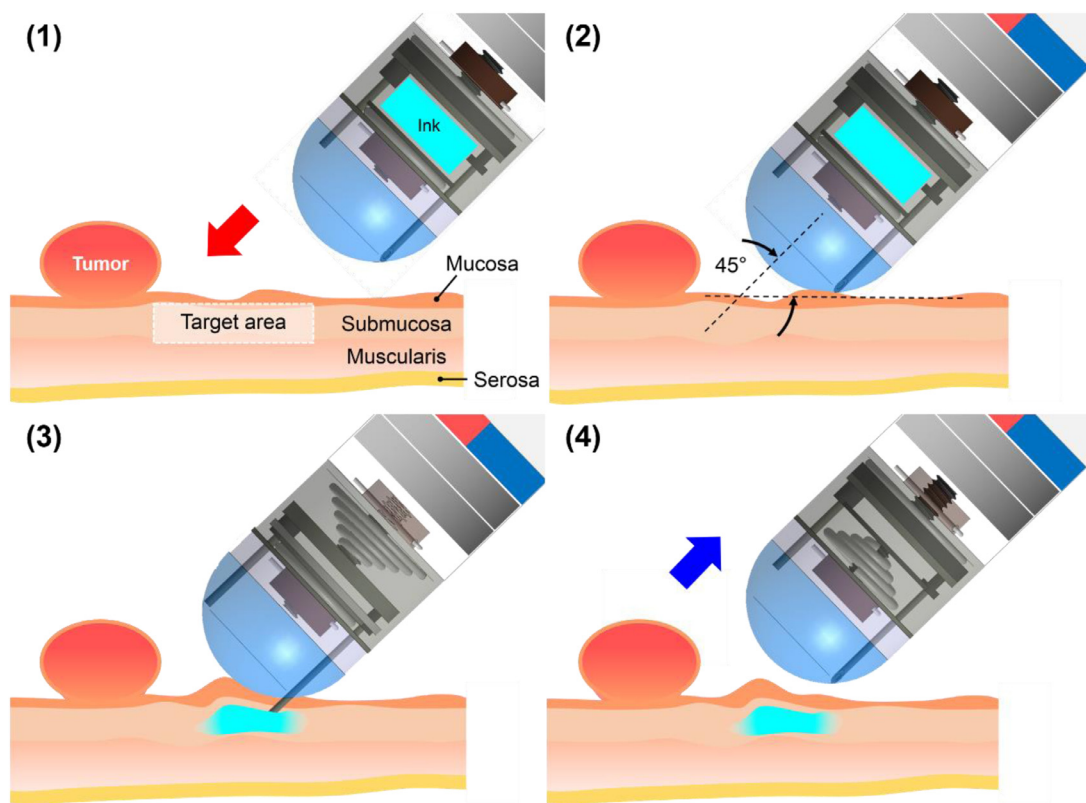


Fig. 2. Working principle of the micro-tattooing device.

three pairs of orthogonal uniform magnetic coils for 3-D alignment, and two pairs of gradient magnetic coils for propulsion [10,14]. Therefore, the CE can be moved by changing the position and the orientation of the magnets in CE relative to the position and orientation of the Helmholtz coil and Maxwell coils in the EMA system. The ALICE also has a reed switch actuated by the EMA system, which is used to activate the triggering mechanism. Based on conditions determined through prior studies of ALICE controls, the tattooing mechanism is designed. Then, we fabricated a micro-tattooing device prototype for use in ex-vivo tests on porcine colon tissue. The working principle of the proposed micro-tattooing device is as shown in Fig. 2 and the detailed operating sequence is as follows;

(1) Each conical spring is fully compressed by the spring holder which is fastened by a nut-shaped piece of Wood's metal. The needle is encased within the capsule casing to prevent damage or per-

foration of the internal colon wall. When the operator finds the target (i.e. tumor, lesion, polyp), the tattooing device installed in the wireless CE is oriented towards the target.

- (2) Next, the CE rotates to a 45° angle from the wall of the colon; which is the same angle used in conventional endoscopic tattooing procedures. Then, the capsule dome is adhered to the colon wall via the EMA control system.
- (3) Once the Wood's metal is melted by the heated Ni-Cr wire, the constrained conical spring #1 deploys and the needle tip reaches the submucosal layer. The needle displacement is limited to 3.3 mm, considering the thickness of the submucosal layer [20,24]. Simultaneously, the tattooing ink of 0.25 ml is loaded into the needle and injected.
- (4) After ink injection, constrained conical spring #2 is deployed by repeating the same process for spring #1: Wood's metal is melted

by the Ni–Cr wire, releasing the opposing spring; completely returning the needle to its original position.

2.4. Conical spring design

To design a conical spring that can generate enough force for the tattooing, the required insertion and injection force should be analyzed when the needle is inserted into the submucosa layer of colon and injects the tattooing ink. Comely, et al. previously investigated the force required to inject ink into adipose tissue of porcine colon and reported it as 5.5 N [26]. However, 5.5 N cannot be used in the conical spring design for our device since the required force can vary depending on the insertion angle and diameter of needle. Accordingly, we experimentally investigate the minimum force required to inject 0.25 ml of tattooing ink into submucosa using a 26G needle with 45° of insertion angle and porcine colon as shown in Fig. 3(a) and (b). The required injection force was measured at 4.967 N (standard deviation 0.929) as shown in Fig. 3(c). The required injection force is investigated according to internal tissue pressure, friction resistance between the silicone seal and spring holder, and miscellaneous forces including tissue viscoelasticity, ink viscosity, and pipe friction according to flow rate. Therefore, we conclude that the tattooing ink can be injected into the submucosa if we employ a conical spring that can generate elastic force more than the measured injection force when it is deployed.

For the actuation sequence to work properly, the minimum force of conical spring #2 should be larger than the maximum force of conical spring #1. Otherwise, conical spring #2 cannot recompress conical spring #1, and the needle cannot be fully withdrawn after the tattooing procedure.

In order to properly design the conical springs, we first analyzed their elastic behavior. A conical spring that is compressing from a free load state shows an elastic and nonlinear behavior before and after a transition point, respectively [27]. The transition force (P_T) is expressed

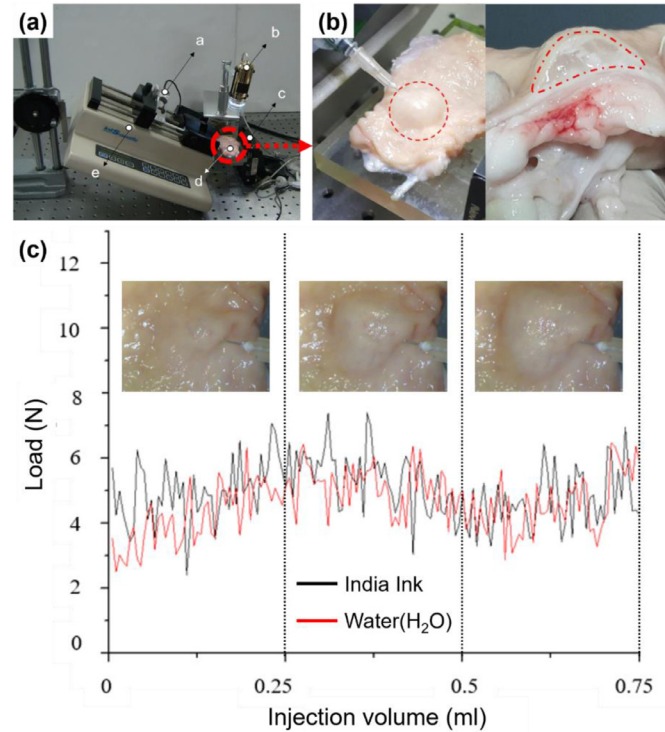


Fig. 3. Experiment results demonstrating the required force to insert needle and to inject ink into submucosa layer: (a) Experiment setup; a. Loadcell, b. Microscope, c. Micro stage, d. Porcine colon, e. Flow regulator, (b) Injected water into porcine colon, (c) Experiment results from load cell.

Table 2

Variables for conical springs #1 and #2.

Nomenclature	#1	#2
D_1 [mm]	3.5	2
D_2 [mm]	9.5	6
n	3	3
n_a	1.2	1.5
d [mm]	0.5	0.6
G [GPa]	72	
L_0 [mm]	10	6.8

as follows.

$$P_T = \frac{Gd^4(L_a - L_s)}{8D_2^3n_a} \quad (1)$$

where, G is shear modulus, d is the spring wire diameter, L_a is the initial active length, L_s is the solid length of active coils, D_2 is the diameter of the largest active coil, n_a means the total number of active coils. Generally, linear and nonlinear intervals of the conical spring can be also defined based on the transition point. Here, the actuations of the proposed mechanism were allowed along the non-linear interval of spring movement because it is deployed from a compressed state. Therefore, the function of length of conical spring with a constant pitch is defined by variation of load as follows [26]:

$$L(P) = L_0 - \left[\frac{2PD_1^4n_a}{Gd^4(D_2 - D_1)} \left\{ \left(1 + \left(\frac{D_2}{D_1} - 1 \right) \frac{n_f}{n_a} \right)^4 - 1 \right\} + (L_a - L_s) \left(1 - \frac{n_f}{n_a} \right) \right] \quad (2)$$

where, L_0 is free length, P is load, D_1 is the diameter of the smallest active coil, n_f means number of free coils. D_2 of the conical spring #1 is determined as 9.5 mm, considering the capsule casing bore diameter, and ASTM A227 spring steel is used to provide adequate needle strength for injection. The elastic force and length calculations of conical spring #1 at a transition point are 2.278 N and 6.038 mm respectively according to Eq. (1) and (2). Conical spring #1 allowed a nonlinear behavior along the range of designed needle displacement (3.3 mm). Accordingly, a theoretical elastic force should be calculated by Eq. (2). The minimal theoretical force at the fully deployed state is calculated at 5.224 N. Based on this theoretical analysis, conical spring #1 is fabricated, and a maximum elastic force at the fully compressed condition is measured at 12.046 N. Using these results, conical spring #2 is designed to generate more force (15 N) at its deployed state than the force (12.046 N) of conical spring #1 at its fully compressed state. Finally, the two conical springs are fabricated as shown in Table 2, and the measured values of elastic force for each conical spring were investigated as shown in Fig. 4.

2.5. Wood's metal-based triggering mechanism

Wood's metal, a liquid metal, can change its material state according to variations in temperature. Accordingly, a mechanism made from the material can be actuated simply and reliably with low power and low conducted heat. Based on the force measurements related to the aforementioned design requirements, we proposed a simple and reliable triggering mechanism which features joule heating of a Wood's metal nut using a Ni–Cr heating wire [28, 29]. The Wood's metal nut is manufactured by fabricating parent metal into a circular disk, drilling a hole at the center, and tapping threads into it.

The triggering mechanism consists of a Wood's metal nut, a Ni–Cr wire, a spring holder and a conical spring as shown Fig 5. A Ni–Cr wire is coiled around the spring holder in a position where it's in contact with the Wood's metal nut. Then, the fully compressed conical spring is secured by fastening the spring holder with the Wood's metal nut. The

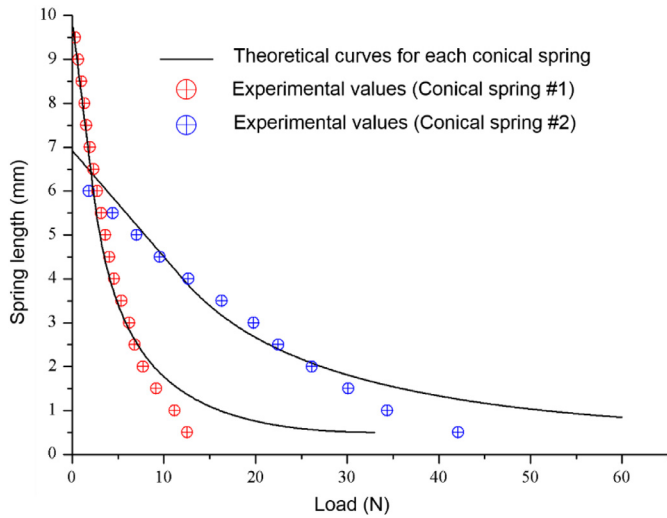


Fig. 4. Experimental results of two conical springs according to displacement.

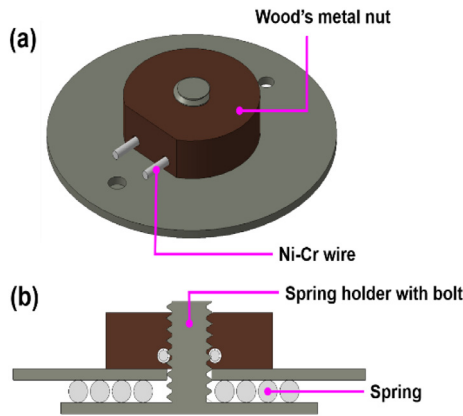


Fig. 5. Schematic design of the triggering mechanism with Wood's metal (a) Isometric view, (b) Section view to show bolt-nut assembly.

resulting size of the overall apparatus occupies only 7.95% of the total capsule volume.

Since the CE's internal volume is limited, the proper height and the thread count for optimization of bolt torque should be determined. The required torque (T_R) to fasten the Wood's metal nut onto the spring holder can be calculated as per the equation below [30].

$$T_R = \frac{F d_m}{2} \left(\frac{l + \pi f d_m \sec \alpha}{\pi d_m - f l \sec \alpha} \right) \quad (3)$$

Table 3
The nominal thread stress of the sample.

Sample No.	The number of threads (height of Wood's metal nut)	Stress (MPa)
1	3 (0.9 mm)	40.18
2	5 (1.5 mm)	24.11
3	7 (2.1 mm)	17.22
4	9 (2.7 mm)	13.39
5	11 (3.3 mm)	10.96

where, F is load, d_m is the mean diameter of thread contact, l is the lead, f is the friction coefficient, and α is the thread angle, measured in the normal plane. The nominal thread stress (σ_B) related to thread parameters can be expressed as follows.

$$\sigma_B = \frac{2F}{\pi d_m n_t p} \quad (4)$$

where, n_t is the number of engaged threads and p is the pitch length.

Furthermore, the nominal thread stress should be lower than the yield strength of the material in order to ensure the threads are structurally stable. Because the nominal thread stress varies according to the number of threads, five samples are studied with various nut heights of 0.9, 1.5, 2.1, 2.7 and 3.3 mm. At a pitch of 0.3 mm (M 1.4), the different nut heights generated thread counts of 3, 5, 7, 9 and 11, respectively. Using the Eq. (4), the acting stress on each thread of the Wood's metal nut is calculated as shown in Table 3, when the restoring force of the conical spring is 71.01 N (wire diameter=0.6 mm, total diameter=8 mm). Therefore, Samples 2–5 would be stable considering a Wood's metal yield strength of 26.20 MPa [31]. Only Sample 1 would fracture when the Wood's metal nut is fastened.

We tested and measured the acting force on the Wood's metal nut until its fracture point to confirm prior theoretical results. The fracture force was measured using a load cell (Model CB1-K50, DACELL Co.), and the results were 41.95, 77.29, 85.34, 103.09 and 138.14 N for each sample, respectively. Based on theoretical and experimental analysis, we selected 'Sample 2' which satisfies strength and space efficiency requirements.

After we assume the body of the capsule is ceramic, we estimated the triggering time and temperature distribution of the mechanism by conducting a numerical simulation using a commercial simulation code (COMSOL Multiphysics®). Here, the boundary conditions were applied as in Table 4.

As a result, we confirmed that the heating time required to reach the Wood's metal melting point (72.3 °C) is 1.5 s as shown in Fig. 6(c). Furthermore, we found that the maximum temperature of the ceramic was 29.65 °C, which is lower than human body temperature.

The spring holder is released and actuated by the conical spring after the Wood's metal is fully melted. We recognized that additional energy and a longer than expected heating time are required in order to heat the material beyond the theoretical melting point (latent fusion heat),

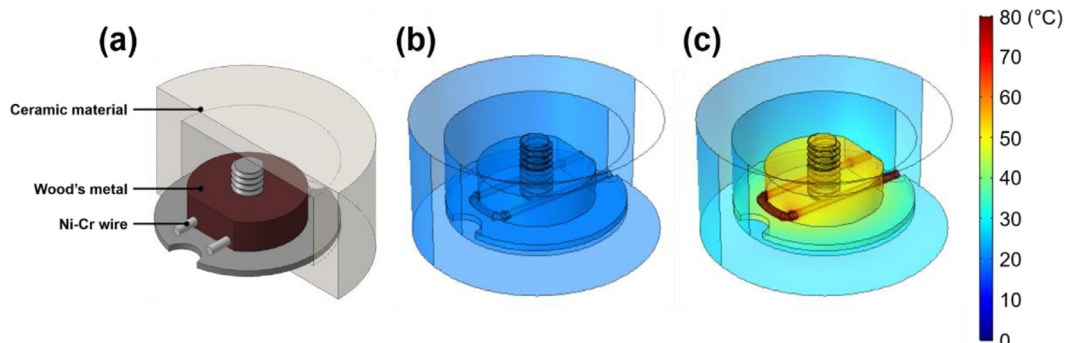


Fig. 6. Simulation results for the temperature distribution (a) Triggering mechanism integrated with capsule body, (b) 0s, (c) 1.5s.

Table 4
Boundary conditions for the numerical simulation.

Parameter	Input condition
Heat Source	Ni-Cr wire
Input Voltage [V]	2.5
Input Ampere [A]	5
Input Power [W]	12.5
Heat Flux	External Natural Convection
Atmosphere [atm]	1
Wood's metal height [mm]	1.5

Table 5
Material properties of Wood's metal [26].

Parameter	Value
Density [kg/m ³]	9700
Coefficient of latent fusion heat [BTU/lbs]	17.2
Volume [mm ³]	24.023

because total melting occurs only after the completing of the phase transition process. Accordingly, the required triggering time should be determined by the heat transfer and thermodynamics. The required electrical energy (Q_E) for melting of the Wood's metal nut is the same as the latent heat of fusion energy (Q_W) [32]. Here, the expected energy consumption for completely changing of material state from a solid to liquid can be derived as follows:

$$Q_W = Q_E \quad (5)$$

$$\rho v L = V I \Delta t \quad (6)$$

where, ρ is density, v is volume, L is the specific latent heat of Wood's metal, V is input voltage, I is input current, and Δt is actuation time.

Also, Eq. (6) can be derived as follow Eq. (7).

$$\Delta t = \frac{\rho v L}{V I} \quad (7)$$

Accordingly, the required electrical energy is defined as a function of time as follows Eq. (7), which allows us to completely estimate the time required for phase transition. The required additional heating time to reach a phase transition was estimated as 1.68 s, using the material properties of Wood's metal shown in Table 5. Therefore, the total triggering time, including both heating and phase transition time, is calculated as 3.18 s.

3. Results

3.1. Triggering mechanism

Also, a triggering test is conducted on a completely assembled triggering mechanism as shown in Fig. 7. As we estimated, Sample 1 was not assembled, and fractured while fastening the Wood's metal nut because the acting force from the conical spring was larger than the yield strength of the material. On the other hand, Samples 2–5 were assembled, and we conducted triggering tests. As a result, when 12.5 W of external input power was applied, each sample was activated within 3.42, 3.89, 3.95 and 6.14 s, respectively. In the case of Sample 2, the triggering mechanism was operated in the shortest time of 3.42 s, and the error rate of triggering time between numerical simulation and experiment results was only 7.55%. Conclusively, we determined that sample 2 is an optimized structure for the proposed triggering mechanism due to the smallest volume and the shortest triggering time.

3.2. Injection test

The proposed tattooing mechanism with triggering mechanism is fabricated, and its practical size is shown in Fig. 8. The inner diameter

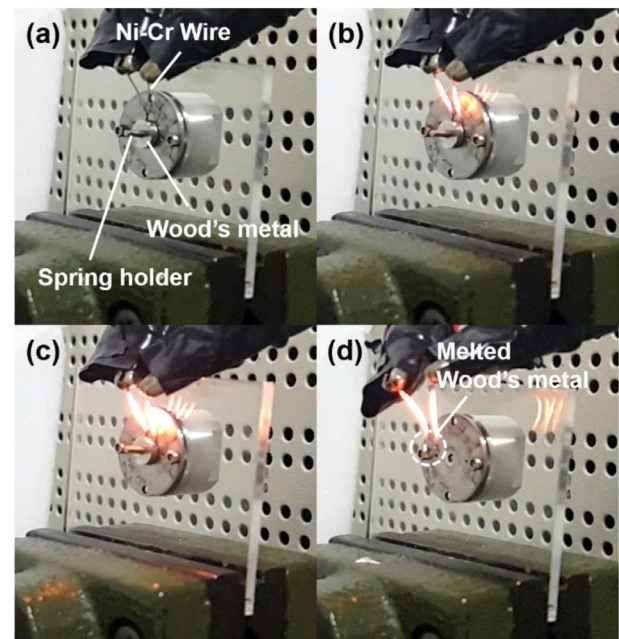


Fig. 7. Triggering test with 1.5 mm-high Wood's metal nut at 1 s intervals.



Fig. 8. Fabricated micro-tattooing device with US five-cent coin (Prototype).

and a thickness of the capsule casing are 11 mm and 5 mm, respectively. Two spring holders include a M1.4 bolt structure and are fabricated from stainless steel. The 26G needle and dummy needle are made using a conventional medical needle.

As shown in Fig. 9(a) and (b), an actuation test without tattooing ink is conducted. First, we coiled the Ni-Cr wire around the Wood's metal and applied 2.5 V. Once the triggering mechanism #1 is initiated, the needle is displaced by the deployment of conical spring #1. We confirmed that the displacement of needle matched the designed stroke (3.3 mm) through visual analysis (Open source motion analysis software *Tracker*). Here, the displacement of the needle is allowed along a longitudinal direction and the needle can penetrate the sub-mucosal layer, without perforating the muscularis layer of the colon. In summary, a Ni-Cr wire in triggering mechanism #2 is heated by Joule heating at 2.5 V. Then, conical spring #2 is deployed, and the needle is returned to its original position along the longitudinal direction

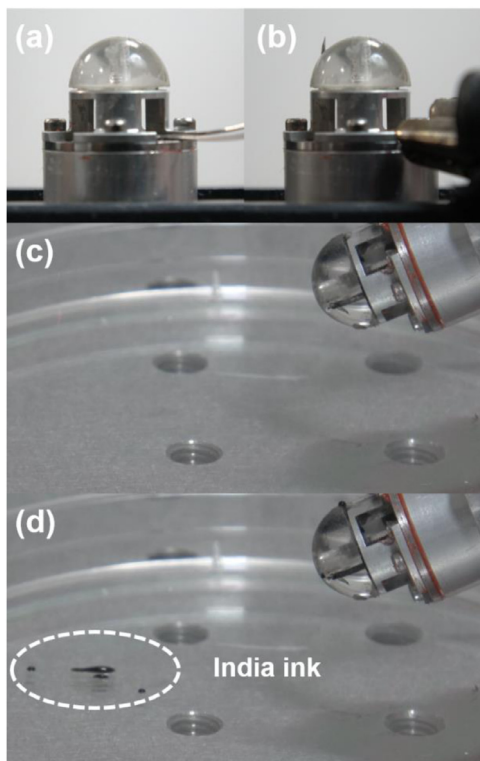


Fig. 9. Performance test of micro-tattooing device (a) Needle insertion test; before activation, (b) Needle insertion of 3.3 mm-displacement, (c) Ink injection test; before activation, (d) India ink injection of 0.25 ml.

in accordance with fully compressing conical spring #1. Each electrical power consumptions of the Ni-Cr wire were 12.375 mWh, respectively. As a result, total amount of power consumption was 24.75 mWh for both injection and withdrawal; consuming 5.21% of total battery capacity (475 mWh).

An in-vitro test of the proposed tattooing mechanism with marking solution (India ink with 0.9% normal saline in a 1:100 dilution) is conducted. To mimic the experimental conditions of conventional tattooing procedures, the experiment was conducted by fixing the device orientation at an angle of 45° as shown in Fig. 9(c). The diluted India ink is injected as shown in Fig. 9(d), which is measured at 0.25 ml according to the displacement of needle. Thus, we confirmed that it satisfied the designed injection capacity. In the same manner, the needle withdrawal is conducted by independent power input to triggering mechanism #2.

3.3. Ex-vivo test on porcine colon

In order to demonstrate the feasibility of the tattooing mechanism, an ex-vivo test using an excised porcine colon is performed. The porcine colon segments are prepared within 12 h after an extraction. The prepared 100 cm² porcine colon segment is extracted from an area near the rectum. Fig. 10(a) and (b) show that the orientation of tattooing mechanism was fixed at an angle of 45° and the completely initiated triggering mechanism #1. After the initiation of triggering mechanism #2 for the needle withdrawal, we hemisected a porcine colon specimen along the injection point. As shown in Fig. 10(c), the marking solution is successfully injected into the submucosal layer of the porcine colon. In addition, we confirmed that there was no perforation on the side opposite the injected area, meaning the designed needle displacement didn't reach a depth sufficient to penetrate the colon wall.

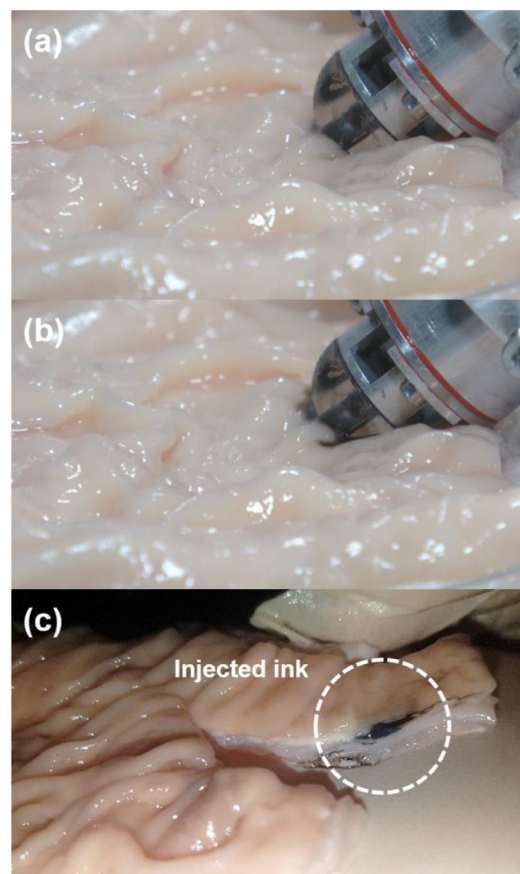


Fig. 10. Ex-vivo test with porcine colon (a) Before activation, (b) Needle insertion and ink injection, (c) injected ink in submucosal layer of porcine colon.

4. Conclusion

We presented a novel micro-tattooing device for the capsule endoscope with low electrical power requirements and a minimized volume. All components are designed to be compatible with a conventional CE enclosure. The needle moves along the longitudinal direction, allowing the surgeon to view the procedure through the camera. Based on our prerequisites, two conical springs are employed to allow space for a 0.25 ml ink cartridge. The conical springs are designed based on the required injection and insertion force. Both conical springs' forces are theoretically analyzed and measured experimentally. To minimize electrical power consumption and reduce the size of the mechanism, a simple yet reliable triggering mechanism using Wood's metal is proposed. The triggering mechanisms can lock and initiate two conical springs. We also confirmed that reaching the melting point of the Wood's metal required relatively small amount of electrical power. In order to make an effective locking and triggering mechanism, a nut-bolt structure was employed between the Wood's metal and spring holder, and the thread count was determined using a nominal stress analysis on the thread surface. The actuation time was analyzed using a numerical simulation and verified by an activation test. To evaluate the feasibility of proposed mechanisms actuation, we confirmed the needle of the tattooing mechanism is displaced up to 3.3 mm along the longitudinal direction and the India ink is injected. We then carried out an ex-vivo test on an excised porcine colon to verify the feasibility of the proposed tattooing device. As a result, the ex-vivo test with the porcine colon indicated that the proposed tattooing mechanism can inject tattooing ink in the proper orientation and depth, and operate with minimal electrical power consumption. The proposed micro-tattooing device using a Wood's metal-based triggering mechanism achieves competitive results, both in terms of power consumption

and the space required relative to the available volume in actual CE devices. In the near future, the proposed tattooing mechanism can be integrated into ALICE with EMA system after optimizing the design and power distribution system. We hope that the proposed micro-tattooing device will be seen as an appealing tool for application in next generation CE devices.

Disclosures

Seonggun Joe, Dongkyu Lee, Hyeonseok Kang, Byungjeon Kang, Jong-Oh Park and Byungkyu Kim declare no conflicts of interest.

Declaration of Competing Interest

The authors declare that they have no known competing financial interests or personal relationships that could have appeared to influence the work reported in this paper.

Acknowledgments

This research was supported by the Next-generation Medical Device Development Program for Newly-Created Market of the **National Research Foundation (NRF)** funded by the Korean government, MSIP (No. 2015M3D5A1065682).

Supplementary material

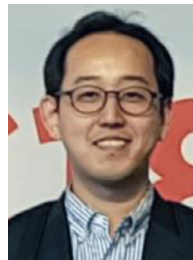
Supplementary material associated with this article can be found, in the online version, at doi:[10.1016/j.mechatronics.2019.102259](https://doi.org/10.1016/j.mechatronics.2019.102259).

References

- Rondonotti E, et al. Small bowel capsule endoscopy in clinical practice: a multicenter 7-year survey. *Eur J Gastroenterol Hepatol* 2010;22(11):1380–6.
- Koulaouzidis A, Rondonotti E, Karargyris A. Small-bowel capsule endoscopy: a ten-point contemporary review. *World J Gastroenterol* 2013;19(3):3726.
- Kwack WG, Lim YJ. Current status and research into overcoming limitations of capsule endoscopy. *Clin Endosc* 2016;49(1):8.
- Gabrieli N, et al. A novel soft device for assisting magnetically-driven soft-tethered capsule navigation. In: 2018 IEEE International Conference on Cyborg and Bionic Systems (CBS). IEEE; 2018. p. 261–5.
- Ciuti G, et al. Frontiers of robotic endoscopic capsules: a review. *J Microbio Robot* 2016;11:1–18.
- Liu L, Towfighian S, Hila A. A review of locomotion systems for capsule endoscopy. *IEEE Rev Biomed Eng* 2015;8:138–51.
- Kim HM, et al. Active locomotion of a paddling-based capsule endoscope in an in vitro and in vivo experiment (with videos). *Gastrointest Endosc* 2010;72(2):381–7.
- Sliker LJ, Kern MD, Schoen JA, Rentschler ME. Surgical evaluation of a novel tethered robotic capsule endoscope using micro-patterned treads. *Surg Endosc* 2012;26(10):2862–9.
- Le VH, et al. Shape memory alloy-based biopsy device for active locomotive intestinal capsule endoscopy. *P I Mech Eng H* 2015;229(3):255–63.
- Lien GS, Wu MS, Chen CN, Liu CW, Suk FM. Feasibility and safety of a novel magnetic-assisted capsule endoscope system in a preliminary examination for upper gastrointestinal tract. *Surg Endosc* 2018;32(4):1937–44.
- He JY, Wu X, Jiang YG, Peng Q, Jain R. Hookworm detection in wireless capsule endoscopy images with deep learning. *IEEE T Image Process* 2018;27(5):2379–92.
- Le VH, Lee C, Go G, Park JO, Park S. Miniaturized biopsy module using gripper tool for active locomotive capsule endoscopy. *Mechatronics* 2017;44:52–9.
- Woods SP, Constandinou TG. A compact targeted drug delivery mechanism for a next generation wireless capsule endoscope. *J Microbio Robot* 2016;11:1–4.
- Woods SP, Constandinou TG. A novel holding mechanism for next generation active wireless capsule endoscopy. In: *Engineering in Medicine and Biology Society (EMBC), 2015 37th Annual International Conference of the IEEE*; 2015. p. 1181–5.
- Yim S, Goyal K, Sitti M. Magnetically actuated soft capsule with the multimodal drug release function. *IEEE/ASME Trans Mechatronics* 2013;18(4):1413–18.
- Le VH, et al. A soft-magnet-based drug-delivery module for active locomotive intestinal capsule endoscopy using an electromagnetic actuation system. *Sensor Actuat A-Phys* 2016;243:81–9.
- Pohl J. Endoscopic tattooing. *Video J Enc GI Endos* 2013;1(2):355–6.
- Kim JH, Kim WH. Colonoscopic tattooing of colonic lesions. *Korean J Gastroenterol* 2015;66:190–3.
- Botoman VA, Pietro M, Thirlby RC. Localization of colonic lesions with endoscopic tattoo. *Dis Colon Rectum* 1994;37(8):775–6.
- Fu KI, et al. A new endoscopic tattooing technique for identifying the location of colonic lesions during laparoscopic surgery: a comparison with the conventional technique. *Endoscopy* 2001;33(08):687–91.
- Hoang Manh Cuong, et al. Intestinal tattooing mechanism integrated with active wireless capsule endoscope. In: 2018 7th IEEE International Conference on Biomedical Robotics and Biomechanics (BIOROB). IEEE; 2018. p. 1254–9.
- Joe S, Lee D, Kang B, Park JO, Kim B. Micro tattooing mechanism for the capsule endoscope. In: *Ubiquitous Robots and Ambient Intelligence (URAI), 2017 14th International Conference on*; 2017. p. 830–1.
- Sadahiro S, et al. Analysis of length and surface area of each segment of the large intestine according to age, sex and physique. *Surg Radiol Anat* 1992;14(3):251–7.
- Huh CH, Bhutani MS, Farfan EB, Bolch WE. Individual variations in mucosa and total wall thickness in the stomach and rectum assessed via endoscopic ultrasound. *Physiol Meas* 2003;24(4):N15.
- Sven K, Josipa F. Interstitial hydrostatic pressure: a manual for students. *Adv Physiol Educ* 2007;31(1):116–17.
- Comley Kerstyn, Fleck Norman. Deep penetration and liquid injection into adipose tissue. *J Mech Mater Struct* 2011;6(1):127–40.
- Rodriguez E, Paredes M, Sartor M. Analytical behavior law for a constant pitch conical compression spring. *J Mech Design* 2006;128(6):1352–6.
- Tambornino F, et al. Electrocrystallization: a synthetic method for intermetallic phases with polar metal–metal bonding. *Inorg Chem* 2016;55(21):11551–9.
- Secareanu R, et al. Experimental and numerical study of freezing and flow characteristics of Wood's metal injection in a water pool. *Appl Therm Eng* 2016;103:1261–77.
- Ochsner A, Altenbach H. *Mechanical and materials engineering of modern structure and component design (Vol. 70)*. Cham: Springer; 2015.
- Kim DG, et al. Evaluation of filler materials used for uniform load distribution at boundaries during structural biomechanical testing of whole vertebrae. *J Biomech Eng* 2006;128(1):161–5.
- Cengel YA. *Thermodynamics: an engineering approach*. McGraw-Hill Higher Education; 2007.



Seonggun Joe received his B.S. and M.S. degrees from Korea Aerospace University, Korea, in 2016 and 2018, respectively. He is currently a PhD candidate at the BioRobotics Institute of the Scuola Superiore Sant'Anna, and Center for Micro-Biorobotics of the Istituto Italiano di Tecnologia (IIT), Pontedera (Pisa), Italy. His-research interests include the bioinspired soft robotics, sensorized soft actuators and bio/medical application robot.



Dongkyu Lee received his PhD in aerospace and mechanical engineering from Korea Aerospace University in 2018. Currently, he works as a postdoctoral researcher at the Space Mechanisms and Robotics Laboratory in Korea Aerospace University. He received his B.S. and M.S. degrees from Korea Aerospace University. His-major research interests include space mechanism, robotics and bio/medical application robots.



Hyeonseok Kang received his B.S. degrees from Korea Aerospace University, Korea, in 2018, and is now in a Master's course at Korea Aerospace University. His-current research interests include robotics and mechanism design for medical device.



Byungjeon Kang received his BS (2008) and MS (2010) degrees in mechanical engineering from the Chonnam National University, Gwangju, Korea, and a PhD (2015) degree in biorobotics from Scuola Superiore Sant'Anna, Pisa, Italy. He is a senior research scientist in the Medical Microrobot Center, Chonnam National University, Gwangju, Korea. His-research interests include microactuator/robot and micromanipulation for biomedical applications.



Jong-Oh Park received his BS (1978) and MS (1981) degrees from the department of mechanical engineering, Korea, and a PhD (1987) in robotics from Stuttgart University, Germany. Between 1982 and 1987, he worked as a guest researcher at the Fraunhofer-Institut für Produktionstechnik und Automatisierung (FhG IPA), Germany. He worked as a principal researcher in the Korea Institute of Science and Technology (KIST) from 1987 to 2005, and he was a director of the Microsystem Research Center at KIST from 1999 to 2005. In 2005, he moved to Chonnam National University where he is now a full professor in the School of Mechanical Engineering and a director of the Robot Research Initiative (RRI). His research interests are biomedical microrobots, medical robots, and service robots.



Byungkyu Kim received his PhD. in mechanical engineering from the University of Wisconsin, Madison, in 1997. From 1997 to 2000, he was a technical staff member of Center for X-ray Lithography in the University of Wisconsin where he developed a computer code for thermal modeling of a mask membrane and wafer during beam exposure. From 2000 to 2005, he worked for Microsystem Center of KIST as a principal research scientist. He was in charge of developing a microcapsule-type robotic endoscope. Currently, he is a professor in Korea Aerospace University. His research interests include space mechanism, robotics, micro/nano-manipulator and bio/medical application robots.